

Application of computer simulation to study heat transfer in concrete with different densities

Raniere H. P. Lira¹, Karlisson A. N. Silva²

¹ Universidade Federal de Alagoas, Campus Sertão

Rod. AL 145, Km 3, nº 3849, Cidade Universitária, 57480-000, Delmiro Gouveia – AL, Brasil
raniere.lira@delmiro.ufal.br

² Universidade Federal de Alagoas, Campus Sertão

Rod. AL 145, Km 3, nº 3849, Cidade Universitária, 57480-000, Delmiro Gouveia – AL, Brasil
karlisson.silva@delmiro.ufal.br

Abstract. Thermal comfort in buildings has been researched through new materials that reduce energy consumption. Lightweight concrete appears as an alternative for civil construction as it presents particular characteristics such as lower specific mass and a higher thermal insulation capacity than conventional concrete. The objective of this work was to evaluate the heat transfer process in concretes with different densities using computational modeling. A mathematical model for heat transfer in concrete blocks with different densities was implemented and all simulations were carried out using the Ansys Student 2023 R2 program. Normal Density Concretes (NDC) and Foamy Cellular Concretes (FCC) were produced with two different proportions, one with 10% foam (FCC10) and the other with 20% foam (FCC20), using air-entraining additives to generate foam. The simulation results presented a good representation of the heat transfer phenomenon when compared with the experimental results. They showed that the addition of foam to concrete reduces thermal conductivity, improving energy efficiency in buildings, demonstrating the potential of these materials for applications in civil construction.

Keywords: Thermal conductivity, Foamed Cellular Concrete, Computational Modeling.

1 Introduction

Urban growth around the world has caused a great demand for durable and more efficient buildings, Gao et al. [1]. In this situation, constructions using concrete become a frequent option due to its more economical value when compared to other solutions, its versatility and good mechanical resistance, Oktay et al. [2]. However, the intense use of this material can present obstacles, especially with regard to the use of thermal energy by buildings, which has a major environmental impact.

According to Cao et al. [3], the energy used to heat and cool environments corresponds to 37% of the total energy production in China, the United States and the European Union. To meet this demand, one of the energy sources used is mineral coal, which occupies 25% of this energy matrix, where the burning of this product releases greenhouse gases, Deng et al. [4], Gielisch and Kropp [5]. In Brazil, data provided by the Ministry of Mines and Energy, through the national energy balance (2022), indicate that residential consumption (heating, refrigeration, lighting, among others) is responsible for 26.4% of the demand for all national production of energy and coal consumption represents 3.9% of the energy matrix.

Thermal comfort in buildings has been researched through new materials that reduce energy consumption. Lightweight concrete appears as an alternative for civil construction as it presents particular characteristics such as lower specific mass, acoustic performance and thermal insulating capacity when compared to traditional concrete, as pointed out by Sacht et al. [6].

The types of concrete most studied by researchers can be obtained by replacing natural coarse aggregates with different types of additions, such as: airgel, rubber aggregates, expanded clay, fly ash, perlite, expanded polystyrene and expanded glass, Silva et al. [7].

Other types are lightweight concrete using air-entraining additives. The addition of these types of additives to concrete during its production promotes the formation of microbubbles distributed homogeneously in the cement matrix, Tayeh et al. [8].

The evaluation of concrete porosity can be carried out in accordance with NBR 9778 [9], evaluating the real specific mass, also known as absolute density.

Lightweight concrete has a wide range of uses in the industry in prefabricated elements, Antunes et al. [10]. In homes, residential and commercial buildings, in the manufacture of structural elements such as slabs and walls, according to Gomes et al. [11], the author's state that it is very important to measure heat transfer between the external and internal environment of buildings, aiming at rational energy consumption and thermal comfort for its users. For Kim et al. [12], humidity is one of the main factors that affect the thermal conductivity of concrete, since, when cured wet or dry, it affects the chemical reactions of the cement.

The objective of the present work was to evaluate the heat transfer process in concretes with different densities, produced with air-entraining additives, using computational modeling.

2 Mathematical model

The temperature distribution in an isotropic and homogeneous medium, for Cartesian coordinates, is obtained from the energy conservation equation, resulting in the heat diffusion equation, Eq. (1) Incropera et al. [13], Çengel and Ghajar [14].

$$\frac{\partial^2 T}{\partial x^2} + \frac{\partial^2 T}{\partial y^2} + \frac{\partial^2 T}{\partial z^2} + \frac{\dot{q}}{k} = \frac{\rho c_p}{k} \frac{\partial T}{\partial t}. \quad (1)$$

Where T is the temperature (K), \dot{q} is the energy generation rate per unit volume of the medium (W/m^3), k the thermal conductivity of the medium ($\text{W}/\text{m}\cdot\text{K}$), ρ is the specific mass (kg/m^3), c_p is the specific heat ($\text{J}/\text{kg}\cdot\text{K}$) and t the time (s), Incropera et al. [13], Çengel and Ghajar [14].

The thermal conductivity k , indicates the amount of heat that can flow through the solid body, is defined according to Fourier's Law according to Eq. (2), Kreith and Bohn [15].

$$k = \frac{q/A}{\nabla T}. \quad (2)$$

Where q is the heat transfer rate (W), A is the area perpendicular to the heat transfer (m^2) and ∇T the temperature gradient.

The thermal resistance R_T (K/W), corresponds to the resistance that a wall offers to the heat flow by conduction, is defined in Eq. (3), Incropera et al. [13], Kreith and Bohn [15].

$$R_T = \frac{\Delta T}{q} = \frac{L}{kA}. \quad (3)$$

Solving the heat diffusion equation provides the variation in temperature in relation to space and time. Considering a semi-infinite solid with transient one-dimensional heat conduction, without heat generation source and appropriate conditions, initial $T(x,0) = T_i$ and boundary $T(0,t) = T_i$ and $T(x \rightarrow \infty, t) = T_i$, applied in Eq. (1) for a constant thermal flux on the surface, as per the specified literature results in in Eq. (4), Incropera et al. [13], Kreith and Bohn [15].

$$T(x,t) - T_i = \frac{2q(\alpha t / \pi)^{1/2}}{k} \exp\left(\frac{-x^2}{4\alpha t}\right) - \frac{qx}{k} \operatorname{erfc}\left(\frac{x}{2\sqrt{\alpha t}}\right). \quad (4)$$

Where x is the length (m) and t is the time (s). The results from Eq. (4) can be used to construct temperature histories showing the transient temperature distribution.

3 Case Description

To validate and test the mathematical model used in the simulations, tests were carried out on a prismatic concert block similar to that used by Silva et al. [7]. The block used in the simulation had dimensions of a total length of 0.17 m, width and height of 0.10 m, respectively. The geometry of the concrete block is shown in Fig. 1.

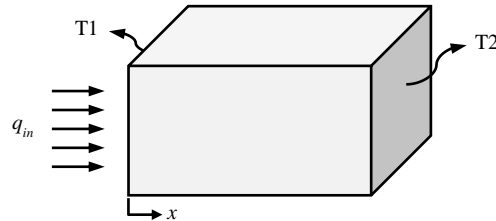


Figure 1. Geometry used in the simulation.

The representative mesh of the numerical model was constructed in the Ansys Mesh Student software, with hexahedral elements with edges measuring 2×10^{-3} m, totaling 212500 elements and 223686 nodes.

The simulations were carried out considering one-dimensional conduction in a transient regime with time step 300 s, without sources of internal heat generation and with constant properties, with the help of the Ansys-CFX software in the academic version, with a convergence criterion of 10^{-8} in relation to the RMS (Root Mean Square) residual error, Ansys Student 2023 R2 [16].

The initial and boundary conditions were defined according with the same conditions used by Silva et al. [7]:

$$\begin{aligned} T &= T_i(x) \quad \text{at } t = 0 \quad \text{for } 0 \leq x \leq L. \\ T &= T_1 \quad \text{at } x = 0 \quad \text{for } t > 0. \\ T &= T_2 \quad \text{at } x = L \quad \text{for } t > 0. \end{aligned}$$

On the front face, a constant heat flux of 643 W/m^2 was specified. On the back face, it was specified as heat transfer by natural convection to the environment with an average temperature of approximately 305.15 K.

On the side, top and bottom surfaces of the block, thermal insulation conditions were applied.

In the simulations, concrete with three different densities was specified as the block material, according to the types of concrete produced by Silva et al. [7], being: Normal Density Concrete (NDC) and Foamy Cellular Concrete (FCC) with two different proportions, one with 10% foam (FCC10) and the other with 20% foam (FCC20), using air-entraining additives to generate foam.

The physical and transport properties of the types of concrete were specified according to the results of Silva et al. [7], presented in Table 1.

Table 1. Specific mass and thermal conductivity for different types of concrete, Silva et al. [7].

Concrete	ρ (kg/m ³)	k (W/m.K)
NDC	2380	1.75
FCC10	1730	1.11
FCC20	1510	0.72

4 Results and discussion

In the cases studied, a semi-infinite solid was considered with a constant heat flux on the front face and on the back face convective transfer to the environment.

Figures 2 to 4 show the results obtained by the computational model developed in the present work compared to the experimental results presented by Silva et al. [7].

Figure 2 shows the temperature variation on the front T1 (upper curve) and back T2 (lower curve) faces, for NDC concrete. A good fit is observed between the simulation temperature results in relation to the results of the work by Silva et al. [7].

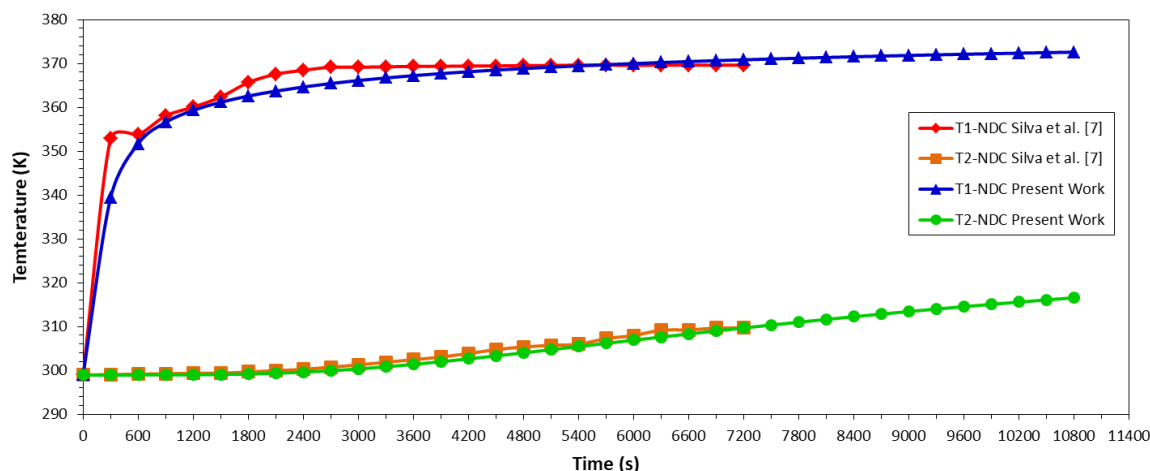


Figure 2. Variation of T1 and T2 temperatures over time, for NDC concrete.

In Fig. 2 it can be seen that initially there is a significant increase in the temperature T1, due to the heat flux applied to the front face of the concrete block, which continues to increase smoothly for an intermediate time interval, tending towards stability over time. On the back face of the block, the variation in temperature T2 occurs with less intensity, showing changes only after a longer period of time. This behavior occurs due to the heat transfer process through the specimen. With the prolongation of the exposure time to the heat source, stability is observed for temperatures T1 and T2, indicating a tendency to reach the steady state, both for the experimental data and for the numerical results.

The same behavior for the variation of temperatures T1 and T2 over time was verified for FCC10 and FCC20 concretes, as can be seen in Fig. 3 and Fig. 4, respectively.

In all cases analyzed, at the end of the simulations there is a difference between the temperatures T1 and T2, as expected for the heat transfer process through a wall. This temperature difference is explained by the resistance that the medium offers to energy transport.

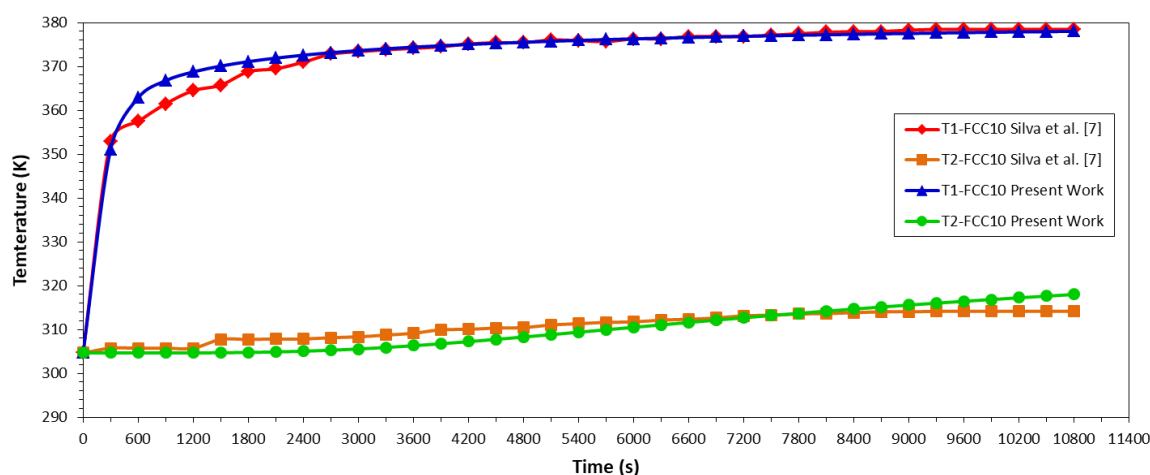


Figure 3. Variation of T1 and T2 temperatures over time, for FCC10 concrete.

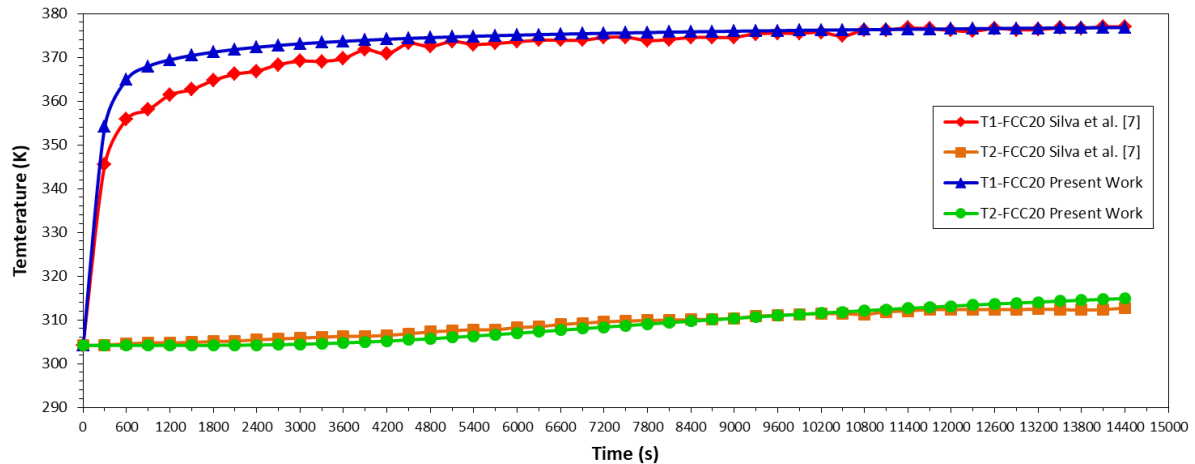


Figure 4. Variation of T1 and T2 temperatures over time, for FCC20 concrete.

Figure 5 shows the temperature distribution simulated for NDC, FCC10 and FCC20 concretes for a time of 7200 s. In all cases, a decrease in temperatures is observed along the length of the concrete blocks. This decay occurs due to the thermal resistance of each of the types of concrete used to manufacture the blocks. According to Incropera et al. [13] and Çengel and Ghajar [14], the thermal resistance to heat conduction in a flat wall is a function of the length, the area through which heat is transferred and the material property called thermal conductivity.

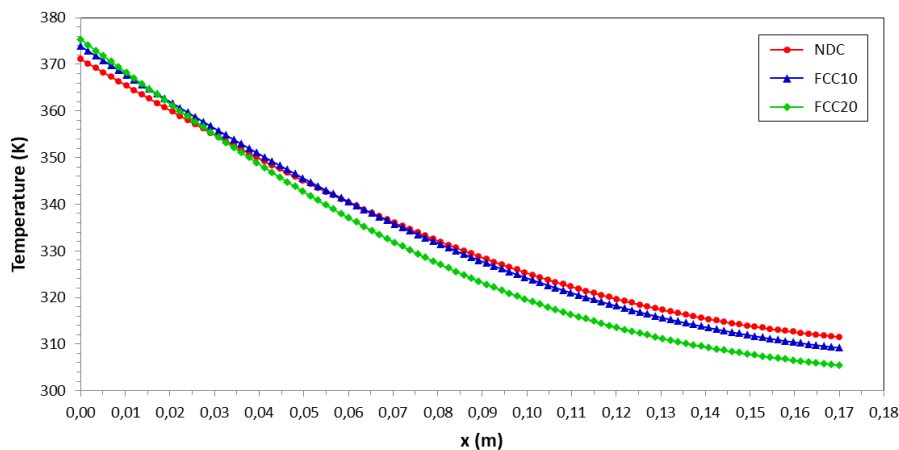


Figure 5. Temperature distribution simulated for NDC, FCC10 and FCC20 concretes (7200 s).

Analyzing Fig. 5, the highest values correspond to the temperature of the front face of the block T1 ($x = 0$ m), the surface that receives the heat flow, and the lowest values correspond to the temperature T2 of the opposite face of the block ($x = 0.17$ m). Taking the T2 temperature, we have temperatures of 311.10 K for the NDC, 309.17 K for the FCC10 and 305.47 K for the FCC20. Maintaining the same boundary conditions, the lower density concretes FCC10 and FCC20 presented lower T2 temperatures when compared to the normal density concrete. These results showed that the FCC10 and FCC20 concretes have a greater resistance to heat transfer, being greater for the FCC20 with a thermal resistance of 23.61 K/W, the FCC10 with an intermediate resistance of 15.31 K/W, with the concrete NDC has the lowest thermal resistance, with 9.71 K/W.

Figure 6 illustrates the temperature contours for the concrete blocks: (a) NDC, (b) FCC10 and (c) FCC20, respectively, for a time of 7200 s. The images clearly demonstrate the behavior of temperature variation in the specimen, from the highest temperature region to the lowest, as a consequence of heat being transferred in the direction of decreasing temperature.

According to the images, the displacement of the temperature field in the test specimen caused by the thermal resistance of the concretes can be observed, with the NDC concrete, with lower thermal resistance,

presenting a temperature difference ΔT of 59.58 K. For the concretes with greater thermal resistance, the temperature difference was 64.68 K for FCC10 and 69.87 K for FCC20.

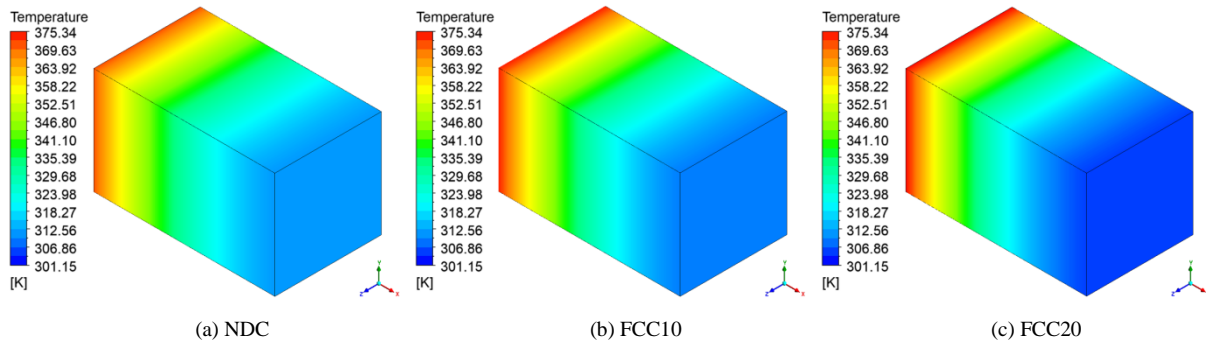


Figure 6. Temperature contours for concretes: (a) NDC, (b) FCC10 e (c) FCC20, (7200 s).

Figures 7 and 8 present the simulation results for different time intervals compared to the steady state, of the temperature distribution for the FCC10 and FCC20 concretes, respectively.

For the types of concrete and in all simulated time intervals, it is observed that the temperature gradually decreases along the length of the concrete blocks. With an increase in the exposure time to the heat source, it is possible to notice a tendency for the curves representing the transient regime to approach the temperature profile corresponding to the steady state, a situation that occurs when the time of exposure to heat tends to infinity. Therefore, the results presented are in agreement with temperature distribution profiles found in the literature.

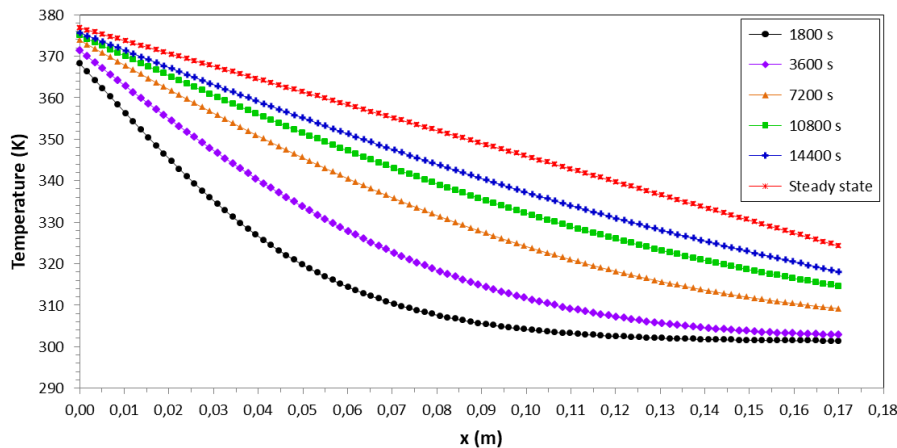


Figure 7. Temperature history simulated for FCC10 concrete.

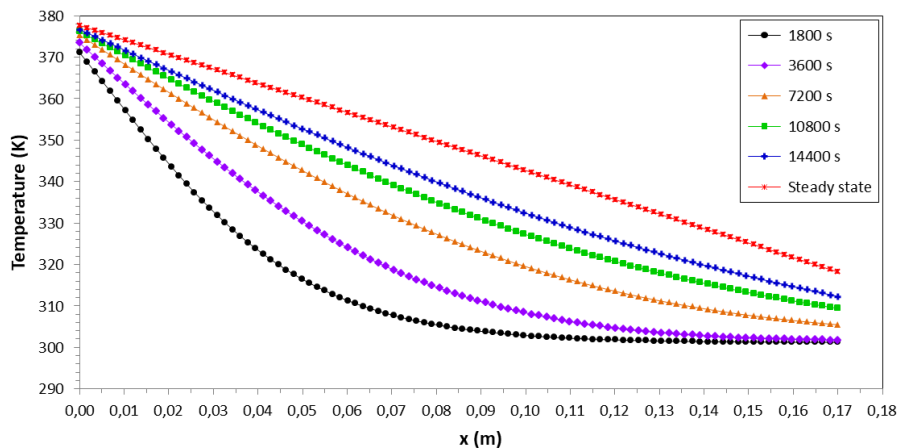


Figure 8. Temperature history simulated for FCC20 concrete.

5 Conclusions

The results presented in this work were satisfactory, where the simulation results presented a good representation of the transfer phenomena involved in the process, being important as a starting point for modeling heat transfer systems.

The results of the simulations proved to be suitable for the purpose of the research, where it was possible to evaluate the heat transfer process in concretes with different densities using computational fluid dynamics.

The results of the proposed model were verified with experimental data and the process evaluation was carried out using temperature profiles, demonstrating a good agreement between them.

NDC concrete presented lower thermal resistance (9.71 K/W) than concretes that received air-entraining additives, generating foam. FCC10 concrete had an intermediate resistance (15.31 K/W), while FCC20 concrete had greater thermal resistance (23.61 K/W).

The addition of foams in different proportions reduces the specific mass, as well as the thermal conductivity of concrete, increasing thermal resistance, which leads to an improvement in energy efficiency in buildings, demonstrating the potential of these materials for applications in civil construction.

Acknowledgements. The authors would like to thank the Federal University of Alagoas – Campus Sertão, for the support in developing and carrying out this work.

References

- [1] Gao, T., Jelle, B. P., Gustavsen, A., Jacobsen, S., Aerogel-incorporated concrete: An experimental study. *Construction and Building Materials Journal*, 2019.
- [2] Oktay, H., Yumrutas, R., Akpolat, A., Mechanical and thermophysical Mechanical and thermophysical. *Construction and Building Materials Journal*, 2015.
- [3] Cao, X., Dai X., Liu, J., Building energy-consumption status worldwide and the state-of-the-art technologies for zero-energy buildings during the past decade. *Energy and Buildings*, pp 198–213, 2016.
- [4] Deng, Y., Wang, C. P., Xiao Y., Chen, H. L., Deng, J., Du, Y. X., Bai, G. X., Effect of greenhouse gases emissions from coal spontaneous combustion under different inerting conditions in the quenching process. *Journal of Thermal Analysis and Calorimetry*, 148:4883–4895 <https://doi.org/10.1007/s10973-022-11936-x>, 2023.
- [5] Gielisch, H., Kropp C., Coal fires a major source of greenhouse gases- a forgotten problem. *GmbH & Co. KG, Germany, Am Technologiepark 1, 45307 Essen, Germany*. ISSN: 2529-8046, 2017.
- [6] Sacht, H. M., Rossignolo, J. A., Santos, W. N., Avaliação da condutividade térmica de concretos leves com argila expandida. *Revista Matéria*, v. 15, n. 1, pp. 031 – 039, 2010.
- [7] Silva, K. A. N., Pinheiro, K. K. B., Lira, R. H. P., Teles, V. L. G., Gomes, P. C. C., Study of Thermal Conductivity in Cellular Concretes, *International Journal of Advances in Engineering & Technology Vol. 17*, Issue 1, pp. 72-82, 2024.
- [8] Tayeh, B., Hakamy, A., Amin, M., Zeyad, A. M., Agwa, I. S., Effect of air agent on mechanical properties and microstructure of lightweight geopolymer concrete under high temperature. *Case studies in construction materials 16* (e00951), 2022.
- [9] NBR 9778, Hardened mortar and concrete - Determination of absorption, void and specific gravity, *ABNT*, 2009.
- [10] Antunes, D., Martins, R., Carmo R., Costa, H., Julio, E., A solution with low-cement-lightweight concrete and high durability for applications in prefabrication. *Construction and Building Materials*. <https://doi.org/10.1016/j.conbuildmat.2020.122153>, 2021.
- [11] Gomes, M. G., Flores-Colen, I., Manga, L.M., Soares, A., Brito, J., The influence of moisture content on the thermal conductivity of external thermal mortars. *Construction and Building Materials* <http://dx.doi.org/10.1016/j.conbuildmat.2016.12.16>, 2017.
- [12] Kim, K., Jeon, S., Kim, J., Yang, S., An experimental study on thermal conductivity of concrete. *Cement and Concrete Research* 33, 363-371, 2003.
- [13] Incropera, F. P., Dewitt, D. P., Bergman, T. L., Lavine, A. S., Fundamentos de Transferência de Calor e Massa, 6ª Edição. *Editora LTC*, 2008.
- [14] Çengel, Y. A.; Ghajar, A. J., Transferência de Calor e Massa – Uma abordagem prática. 4ª Edição. *Editora McgrawHill*, 2012.
- [15] Kreith, F.; Bohn, M. S., Princípios da Transferência de Calor. *Editora Cengage*, 2003.
- [16] Ansys-CFX 23 R2, *ANSYS Tutorials*, 2023.